

Suqi Chen, Zheng Guo, Gaowei Jia, Duoneng Liu

College of Aerospace Science and Engineering, National University of Defense Technology, Changsha, Hunan, 410073, China

Abstract

The paper conducts a study on the flow characteristics of distributed propulsion systems. The layout parameters of the distributed propulsion system are designed as dimensionless, and the primary focus is on the aerodynamic performance of the distributed propeller under different distributed propeller spanwise distance and multi angles of attack. Based on the experimental validation of the numerical simulation method, a high-fidelity quasi-steady RANS simulation is performed on the aerodynamic characteristics of the coupled configuration of distributed propeller-wing-flap using the Multiple Reference Frame (MRF) method. The results show that under a small spanwise distance, the additional tip vortex generated will reduce the propeller efficiency. But as the angle of attack increases, the propeller efficiency first increases and then tends to flatten. The flow relationship between the angle of attack and the distributed propeller spanwise distance can be divided into three flow states: small, medium, and large spanwise distance. In general, a small spanwise distance is conducive to the lift enhancement of the distributed propulsion system, but the existing results show that there is a relationship between the vertical position and spanwise distance of the distributed propeller, which will be discussed in the following research.

Keywords: Distributed propulsion, RANS, Aerodynamics.

1. Introduction

The aviation industry technology has matured after a long period of development, and major aircraft manufacturers around the world are facing fierce competition. Currently, most companies are committed to increasing their market share by reducing aircraft operating costs and negative environmental impacts, with a focus on reliable propulsion systems, low fuel consumption, aviation flight safety, low noise, and multidisciplinary optimization design to achieve ideal flight requirements. Distributed propulsion technology has become one of the revolutionary solutions for the design of intelligent aircraft in the future[1]. Most all-electric/hybrid-electric aircraft represented by models such as NASA Maxwell X-57 and Airbus E-Fan adopt distributed propulsion technology. Taking the X-57 distributed propulsion aircraft as an example, it is equipped with 12 small propellers on the leading edge of the wing, aiming to significantly increase lift by increasing the dynamic pressure and circulation of the downstream wing under low-speed conditions. The presence of the wing reduces the effective vortex flow downstream of the propeller, further improving propeller efficiency and the induced drag of the wing[2].

Based on previous research, Gohardani[3] has provided a detailed definition of distributed propulsion technology: Distributed propulsion technology is primarily applied to subsonic fixed-wing aircraft, and its propulsion system consists of three or more propulsion units (engines/propellers/other propulsion units). Different aircraft have varying array positions, layout positions, number of propulsion units (ranging from five levels A to E), thrust-to-weight ratio (three levels), etc. If the total thrust distribution can cover a specified area of the fuselage, only one propulsion unit may be required; otherwise, the total thrust needs to be achieved through three or more propulsion units to achieve jet diffusion. In addition to providing propulsion performance, the distributed propulsion system also needs to

provide other additional functions. According to the definition of distributed propulsion technology, the coupling effect between the propeller and the wing is crucial. The propeller, as a traditional propulsion unit that has been active since the last century, has gained new design freedoms with the development of distributed propulsion technology.

Drawing from previous research experience, there should be more significant coupled flow effects between distributed propellers and wings. As a result, researchers have conducted a series of studies on relevant flow mechanisms to provide guidance and theoretical foundations for the optimal design of aircraft. Professor Veldhuis from Delft University of Technology has revealed the coupled flow mechanism between an isolated propeller and wing through numerical simulations and experiments[4-7]. Ameyugo[8] believes that one of the key reasons why distributed propulsion systems can improve the aerodynamic performance of aircraft is that the jets from the distributed propellers can uniformly fill the wake of the aircraft's wing, thus optimizing the drag characteristics of the aircraft. Researchers[9-14] have conducted preliminary aerodynamic analyses on the coupled configuration of wings and distributed propellers, verifying the correctness of the computational methods. They have focused on studying the aerodynamic effects of the distributed configuration during the take-off, landing, and cruise phases, such as the interaction between wingtip vortices and propellers. Wang[15] proposed and investigated a propeller-assisted high-lift biplane configuration, which achieved a 2.33% increase in wing lift and a 4.64% reduction in drag compared to a clean wing configuration. The Zhou Zhou team at Northwestern Polytechnical University[16, 17] conducted high-precision quasi-steady numerical simulations (using the MRF method) of the aerodynamic characteristics of low Reynolds number propeller-wing configurations. By analyzing the aerodynamic force coefficients and surface flow field structures of the wing, they revealed the aerodynamic effects of the distributed propeller slipstream on the wing. The study showed that the propeller slipstream increases the total pressure and flow velocity behind the propeller, resulting in an increase in the wing lift. This expansion of the turbulent flow range and the attached flow region on the wing surface was observed, with distinct spanwise distance vortex structures at the boundary of the slipstream area. During the take-off and landing phases, in order to enhance the lift-increasing effect, the distributed configuration is often used in combination with flaps. Researchers[11, 18, 19] such as Viken have conducted numerous numerical simulation studies on the propeller-wing-flap configuration, primarily designing a cruise wing profile with a low-resistance distributed propulsion system and flaps. For this wing profile, they have quantified the lift enhancement effect of the distributed propeller on the wing lift under a 40° flap deflection. Cusati[20] studied the optimal flap deflection angle, gap, and overlap values for distributed propulsion systems to achieve optimal highlift characteristics. Due to the gains from the distributed propulsion system, the take-off length was reduced by 27%, and the author emphasizing the importance of flap design in improving the lowspeed performance of distributed systems.

The layout design parameters such as the number, spanwise distance, and relative position of distributed propellers have a significant impact on the aerodynamic characteristics of distributed propulsion systems. Researchers often utilize high-fidelity CFD numerical simulations to reveal the flow mechanisms. Wang[21] used the RANS method to numerically simulate the impact of different spanwise distance and chordwise positions of propellers above the wing on aerodynamic performance. Beckers[22] studied the interaction between distributed propellers and wings under high-lift conditions (with flaps deployed and high angles of attack). Beckers employed RANS simulations to determine the sensitivity and interaction of design parameters at high angles of attack. Through comparative parametric studies, it was found that the design parameter that had the greatest impact on system performance was the relative vertical position of the propellers with respect to the wings. Significant improvements in propulsion performance could be achieved by tilting the propellers towards the incoming airflow direction and reducing the spacing between them. Propulsive performance could be significantly improved by tilting the propeller downward toward the inflow (by about +30% for $\theta=20$ deg as compared to a nontilted propeller). Researchers such as Rosa[23-26] have conducted multi-fidelity numerical simulation studies and experimental studies on different distributed propeller configurations, mainly focusing on the key factors including the number of propellers, propeller diameter, vertical position of propeller, and flow direction position. Wang[27] studied the flow characteristics of the distributed propulsion system and optimized it: compared with

the basic propeller/wing integration, the distributed propulsion system has a lift-to-drag ratio improved by 21.08% and weakened the average vortex intensity distribution of the propeller flow.

In the past decade or so, the research on distributed propulsion technology has made significant progress from the stage of verifying feasibility to multidisciplinary overall optimization. Most of the previous aerodynamic studies have focused on: how to establish a theoretical aerodynamic model for the distributed propulsion system and conduct preliminary aerodynamic and overall conceptual design; how to use simplified models to quantitatively and qualitatively obtain the aerodynamic characteristics of the distributed propulsion system. There are relatively few studies on the mechanism of bidirectional aerodynamic interference and coupling effects between propeller and wing. Based on the key points summarized above, this paper utilizes CFD methods to conduct a flow mechanism analysis of the distributed propeller-wing-flap model under takeoff and landing conditions, focusing on the coupling effects between different angles of attack and the spanwise distance of distributed propellers. Considering the flow characteristics of distributed layout positions under wide angle of attack. The aim is to provide theoretical guidance for the subsequent optimization design of distributed propulsion systems.

2. Methodology

This study is a CFD numerical simulation analysis of the propeller-wing interaction under the requirement of high lift, aiming to determine the significant aerodynamic effects and sensitivity of the design parameters of the distributed propeller system. The aerodynamic relationship between the angle of attack and the spanwise distance of the distributed propeller is mainly calculated, and the performance of the distributed propeller with different parameters is compared with the results of the aerodynamic characteristics of the wing to guide the follow-up optimization of the wing.

2.1 Geometry

The 2.5D research object of this paper is shown in the Figure 1, which mainly consists of a high-lift wing with flaps and a distributed propeller configuration arranged at the leading edge of the wing. The wing-flap model is based on the method described in Reference [28] and the results of a twosegment airfoil optimization targeting take-off conditions and high lift based on the FX 63-137 airfoil. The propeller used in this study is the APC series electric propulsion propeller 24x12E-PERF with 5 blades. The specific parameters of the distributed propulsion configuration are shown in the Table 1. The distributed propulsion model features a rectangular wing segment with a constant chord length and airfoil. The side boundaries of the wing-flap are periodic boundary conditions, which can effectively simulate the arrangement of an infinite number of propellers on a wing segment of infinite span. Using periodic boundary conditions for the side boundaries of the wing-flap implies that the distributed propellers are rotating in the same direction, while the use of symmetric boundary conditions would indicate counter-rotation. This study investigates the relationship between the angle of attack and the distributed propeller spanwise distance ΔZ_{tip} (expressed as a percentage of the diameter of adjacent propellers), and analyzes its flow mechanism characteristics in detail. The numerical simulation method adopted in this paper is the Multiple Reference Frame (MRF) method. Fully turbulent steady-state Reynolds-averaged Navier-Stokes (RANS) equations were solved with the $K-\omega$ SST (Shear Stress Transport) turbulence model To ensure a y⁺ value of approximately 1, the height of the first grid layer on the solid wall is set at 1e-5m. The model is discretized using hexahedral grid generation, and a schematic diagram of the grid is presented in Figure 1. The flight condition calculated in this paper is for the takeoff phase, with an incoming flow velocity of 32 m/s and a flight altitude of 0 km.

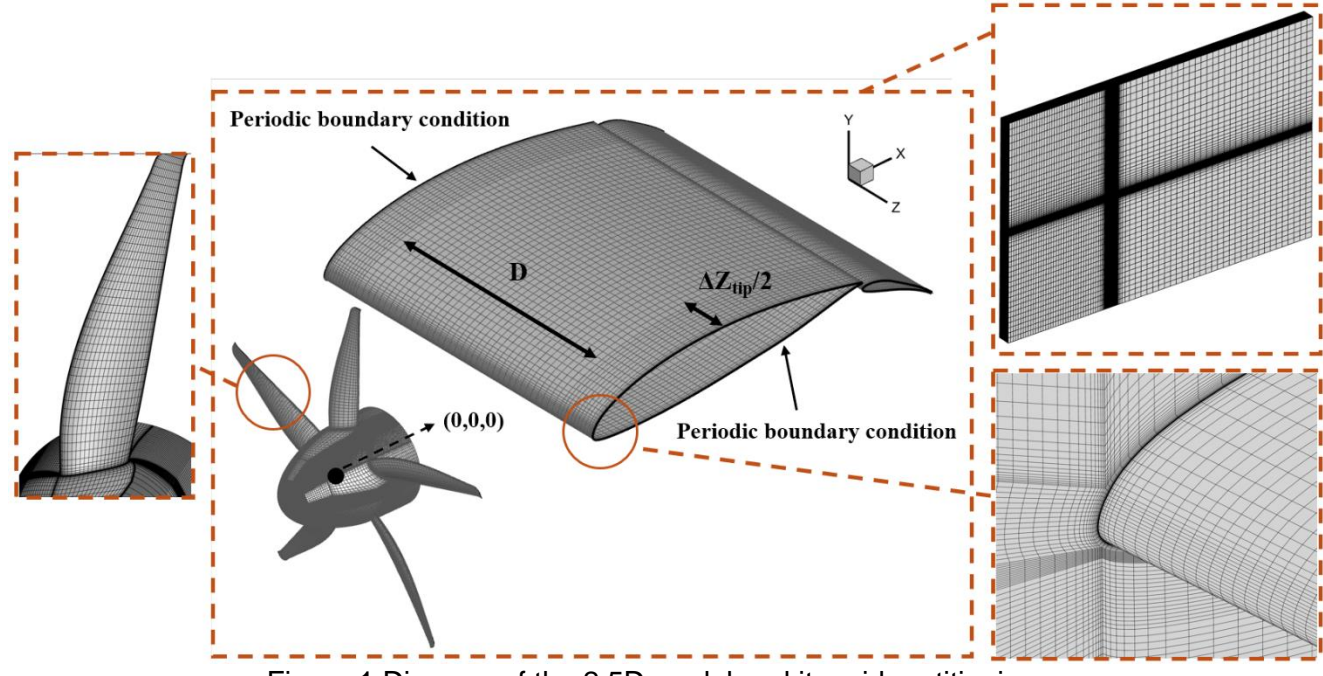


Figure 1 Diagram of the 2.5D model and its grid partitioning

Table 1 Specific parameters of the distributed propulsion configuration (default setting)

Description	Value
Wing Chord(m)	0.7176
Wing Area(m ²)	0.447
Number of Propeller Blades	5
Propeller Diameter(m)	0.6096m
Hubs Diameter	0.1585m

2.2 Grid Dependence Verification

The numerical computational model for the distributed propulsion configuration is divided into a moving domain (propeller) and a static domain (wing-flap). This study conducts a grid independence verification by varying the number of grid cells in local refinement regions of the propeller and the wing/flap separately. The evaluation metrics for the propeller and the wing/flap are the thrust coefficient and the lift/drag coefficient, respectively. The results of the grid independence study are presented in Table 2, Table 3. Taking into account both the capture of flow field details and computational efficiency, the final total grid count for the distributed propulsion model (moving domain + static domain) is determined to be approximately 8 million cells. After computational iterations, the fluctuation range of the monitored values is approximately 0.1%, which can be deemed as a converged state.

Table 2 Grid independence verification for isolated propeller

Prop cases	Coarse	Moderate1	Moderate2	Refined
Grid number	240w	340w	440w	540w
C_{T}	0.07443	0.06573	0.06539	0.06514

Table 3 Grid independence verification for wing-flap

Wing-Flap cases	Coarse	Moderate1	Moderate2	Refined
Grid number	85w	135w	195w	250w
C_D	0.02326	0.02326	0.02322	0.02324
C _L	1.7013	1.7011	1.7014	1.70140

2.3 Numerical Simulation Results Compared with Experimental Results

To validate the accuracy of the numerical simulation method used, the paper refers to the experimental results reported in Reference[29] The problem was set up in ANSYS Fluent, which was based on a pressure-based, steady, implicit Reynolds-Averaged-Navier-Stokes (RANS) solver. The solver used the k- ω Shear Stress Transport (SST) and Reynolds Stress models for closure between the mesh scale and the eddy dissipation scale. The rotation of the propeller is simulated using the

quasi steady method(Multi-Reference Frame, MRF).

(1) Experimental Verification of Calculation Method for Isolated Propeller Performance

The Reference[29] includes measurements of the propeller thrust coefficient, power coefficient, and propeller efficiency at different advance ratios. The Reynolds number corresponding to the reference length of the propeller diameter is 640000. The propeller thrust coefficient at different Reynolds numbers (R_{eD} =640000 or R_{eD} =470000) was obtained by changing the inflow velocity (30m/s or 40m/s) in the experiment. Figure 2 is a characteristic curve diagram of propellers with different advancing ratios at R_{eD} =640,000. The maximum difference between numerical simulation results and experimental results for different coefficients is about 6%, which meets the requirements of engineering. When the Reynolds number is 470000, the numerical simulation results are still in well agreement with the experimental results.

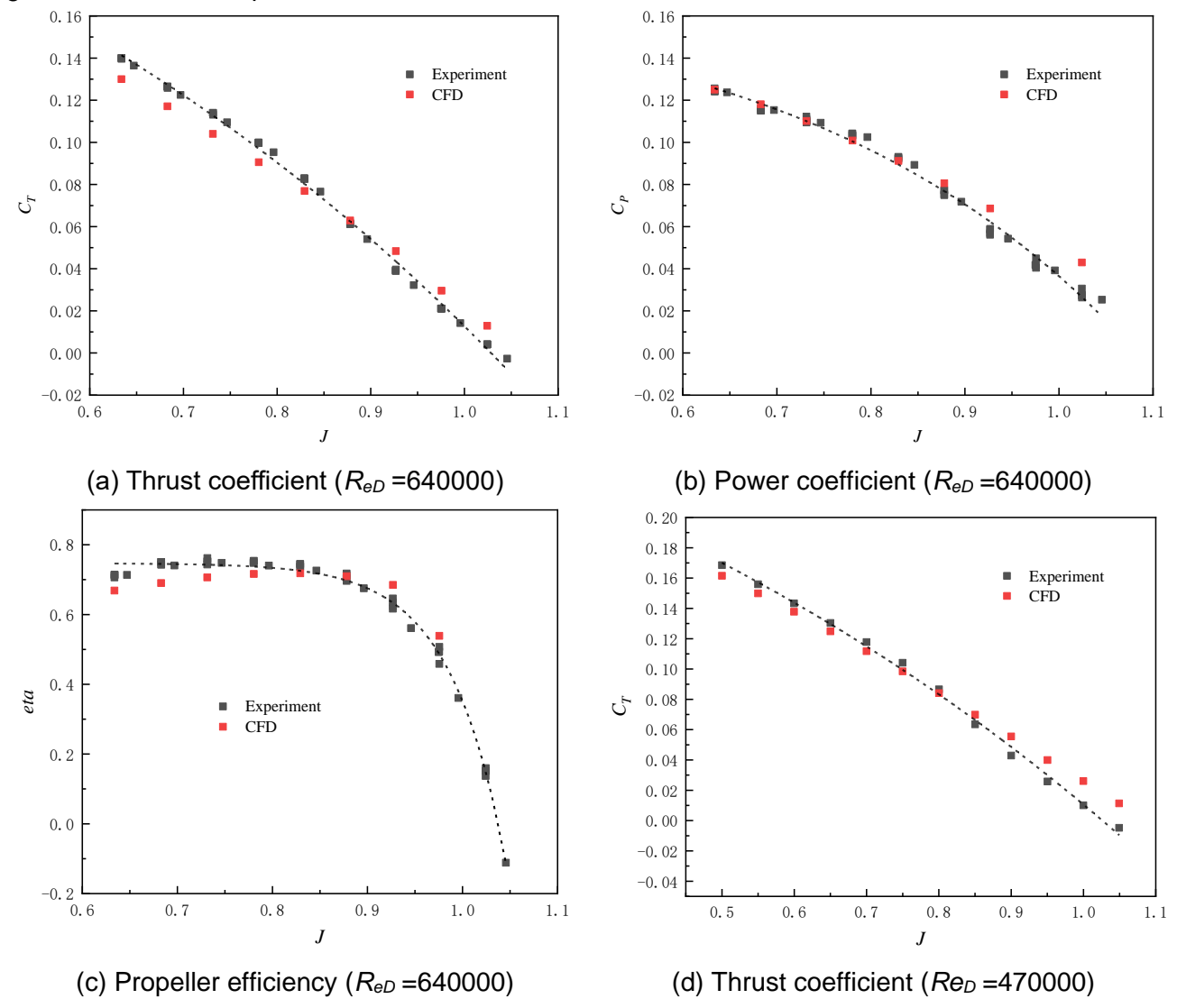


Figure 2 Propeller performance at different Reynolds numbers

(2) Experimental Verification of the Coupling Effect of Wingtip Propeller and Wing with Flaps

The experimental model is a symmetric airfoil with flaps coupled with a propeller at the wingtip. The experimental model uses a wing with a low aspect ratio and a high ratio of diameter to spanwise distance, which facilitates the exhibition of the mechanism of aerodynamic interference between the propeller and wing. The propeller rotates in the same direction as the rotation of the wingtip vortex, and the flap is rotated downward by 10 degrees at this time. The numerical simulation and experimental comparison of lift coefficient and drag coefficient are shown in the Figure 3.

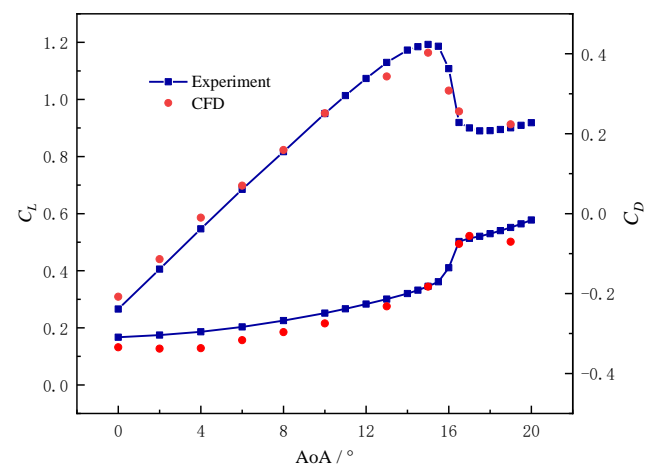


Figure 3 The numerical simulation and experimental comparison of lift coefficient and drag coefficient

3. Studies and Results

3.1 Propeller Performance Study

With a certain takeoff speed determined, not all operating conditions can effectively benefit the distributed propulsion system. As shown in the Figure 4, for the selected 2.5D isolated wing section, the propeller efficiency first increases and then decreases with the increase of the advance ratio. The blocking effect created by the wing in the slipstream significantly increases the pressure behind the propeller. Compared to an isolated propeller, the propeller-wing configuration increases the propeller's thrust coefficient and power coefficient, but the increase in the propeller's thrust coefficient is more significant, resulting in an increase in propeller efficiency. With a fixed inflow velocity, the propeller rotation speed will increase and the wake velocity behind the propeller will also increase as the advance ratio decreases. The lift coefficient of the wing surface presents a quadratic growth trend with the decrease of the advance ratio. When the advance ratio of the propeller is greater than 0.5, the gain in lift generated by the propeller's slipstream on the wing is less than the lift enhancement effect produced by the free inflow on the wing. Considering the propeller efficiency and its lift enhancement effect on the wing, an advance ratio of 0.3 for the propeller is selected for further research.

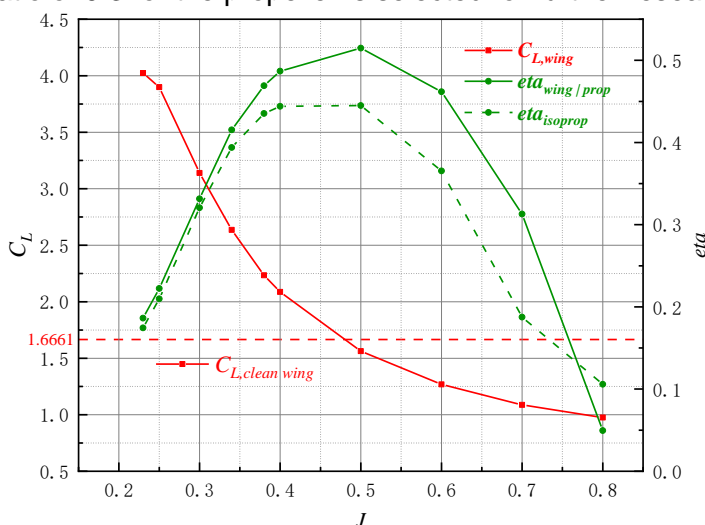


Figure 4 The impact of different advance ratios on propeller efficiency and wing lift coefficient

The propeller layout of the distributed propulsion system is relatively compact, and the coupling effect between distributed propellers is evident. The circumferential induced vortex flow at the tip of distributed propellers affects the performance of individual sub-propellers. Most past studies have focused on analyzing the lift-enhancing effect of propeller slipstreams on airfoils, while fewer studies have revealed the impact of distributed propulsion systems on propeller performance. Figure 5 compares the impact of different angles of attack and ΔZ_{tip} on the propeller efficiency. As the spanwise distance increases, the interaction between distributed propellers is bound to decrease. This study suggests that when $\Delta Z_{tip} = 100\%D$, the mutual interference between propellers is relatively weak. With

the increase in angle of attack, the propeller efficiency of both distributed propeller configurations with ΔZ_{tip} =100%D and ΔZ_{tip} =25%D changes relatively little; When ΔZ_{tip} is small, the propeller efficiency of the distributed propellers first increases and then tends to flatten out as the angle of attack increases. Moreover, as the angle of attack increases, the smaller ΔZ_{tip} results in higher propeller efficiency.

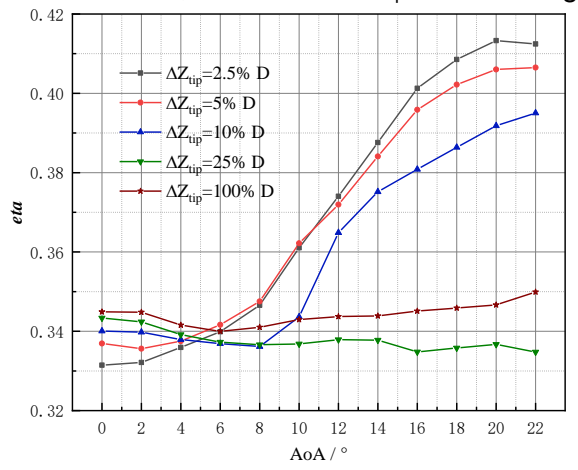


Figure 5 The influence of ΔZ_{tip} on propeller efficiency under different angles of attack

Figure 6 is a schematic diagram of different slice selected for studying flow characteristics: slice Y-Z, slice Z-X. Figure 7 depicts the vortex lines and vorticity distribution under different spanwise distance and angles of attack. When ΔZ_{tip} = 2.5%D, a significant amount of induced vortex structures emerges near the propeller tips due to the interaction between distributed propellers. The viscous dissipation caused by this tip vortex interaction results in a reduction in the propeller efficiency of distributed propellers under low angles of attack. When ΔZ_{tip} = 100%D, the circumferential airflow near the propeller tips is entrained as the blades rotate, and there is no significant vorticity distribution near the tips except for the free vortices escaping from the trailing edges. In this case, the mutual interference between distributed propellers can be neglected. As shown in the Figure 7(a), (c), with the increase in angle of attack, when $\Delta Z_{tip} \le 25$ %D, the circumferential velocity component increases rapidly, enhancing the rotational kinetic energy of the propeller. The induced vortex structures originally present near the propeller tips disappear, resulting in an increase in propeller efficiency.

Figure 8 shows the impact of the distributed propeller spanwise distance and angle of attack on the velocity field of the distributed propulsion system, namely, the velocity vector distribution diagram in the slice Z-X of the computational domain. In Figure 8 (a), the velocity vector profiles are presented when the angle of attack is 0° and ΔZ_{tip} is 2.5%D and 100%D, respectively. The red arrows and black arrows represent the velocity vector distributions of ΔZ_{tip} =100%D and ΔZ_{tip} =2.5%D. The larger ΔZ_{tip} velocity vectors (red) exhibit a significant spanwise component due to the contraction of the slipstream flowing through the propeller, while the smaller ΔZ_{tip} velocity vectors (black) show no obvious spanwise contraction flow in the upstream flow field that should have been generated by the propeller interaction. Figure 8 (b) depicts the velocity vector profiles at different angles of attack with a fixed ΔZ_{tip} . It can be observed that as the angle of attack increases, there is also a significant spanwise flow (pink).

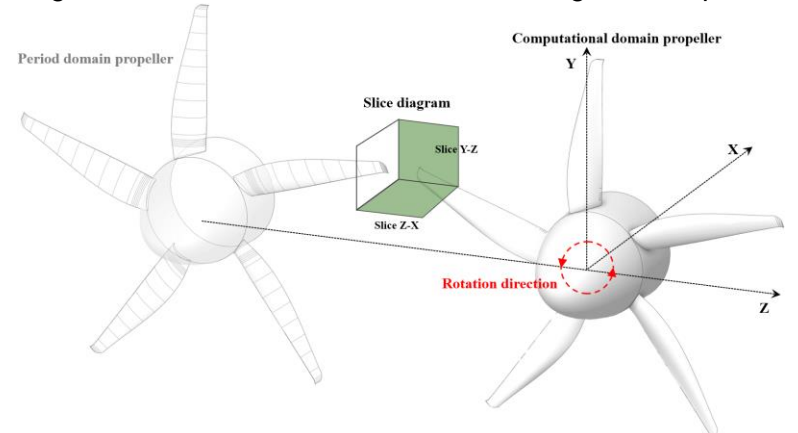


Figure 6 Schematic diagram of slice Y-Z and slice Z-X

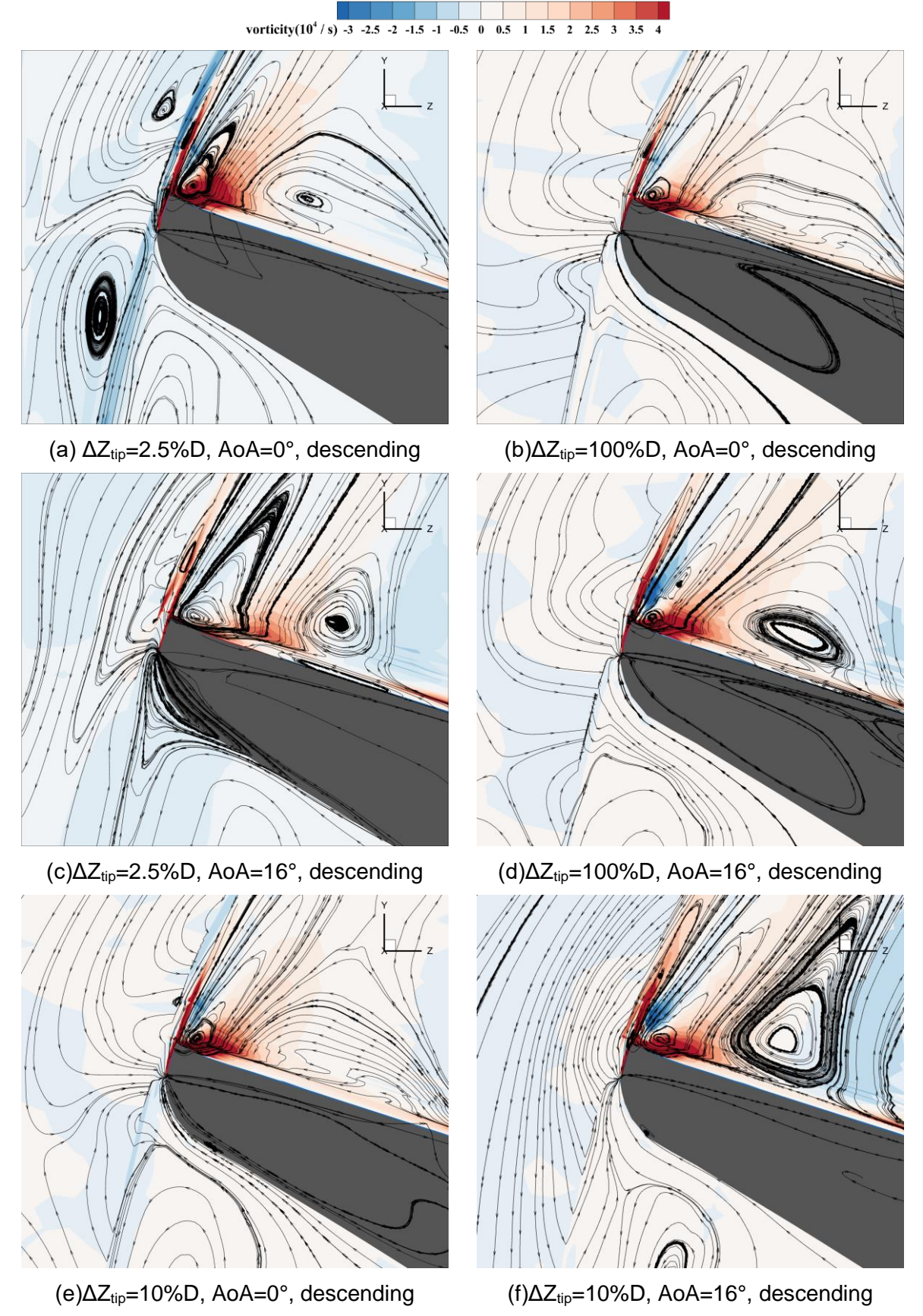
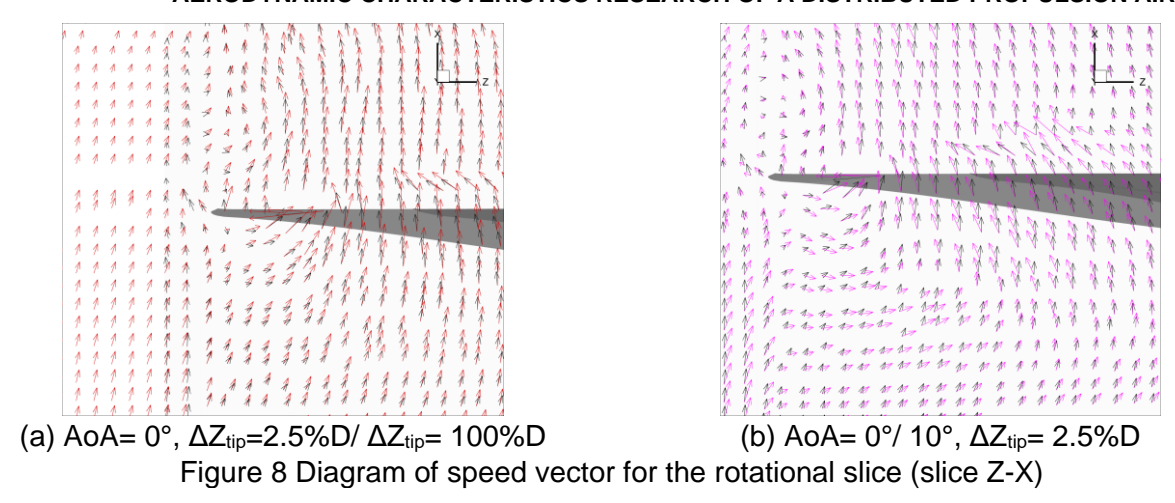
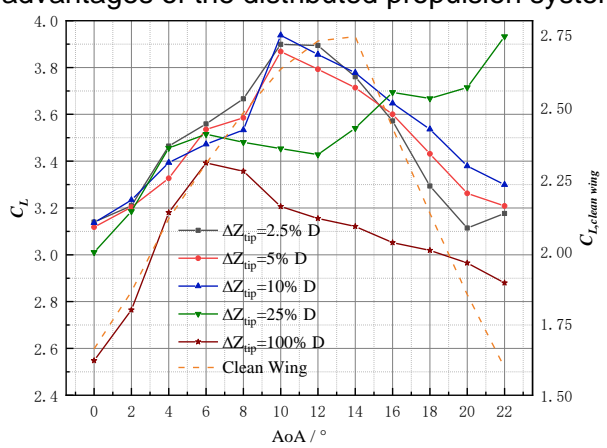


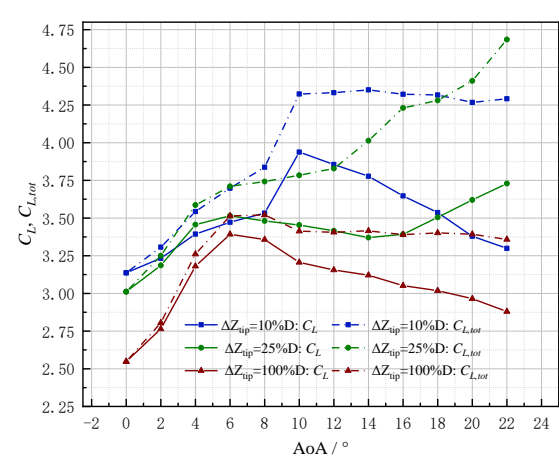
Figure 7 Vortex distribution near the blade tip under different ΔZ_{tip} and angles of attack (slice Y-Z)



3.2 Correlation Between Angle of Attack and Distributed Propeller Spanwise Distance

During takeoff and landing, to achieve optimal lift augmentation, the distributed propellers inevitably interact with the wing-flap system under an angle of attack. This section studies the variation between the angle of attack and the spanwise distance of the distributed propellers (ΔZ_{tip}), aiming to reveal the lift augmentation and flow mechanisms on the wing-flap surface under the influence of slipstream. The Figure 9 (a) uses the curve of the clean wing's lift coefficient varying with the angle of attack as a reference to demonstrate the lift augmentation effect of distributed propulsion and the flow separation point of the clean wing. Therefore, a dual Y-axis is introduced to plot the curves. It can be observed that the flow separation points of different distributed propulsion configurations occur earlier compared to the clean wing, but all ΔZ_{tip} configurations exhibit lift augmentation. When ΔZ_{tip} < 25%D, the flow separation point advances from 14° to 10° angle of attack, and the lift coefficient varies consistently with the angle of attack. The lift coefficient of the wing with distributed propulsion can increase by up to 50% compared to the clean wing. However, when $\Delta Z_{\text{tip}} > 25\%D$, the flow separation point advances to 6° angle of attack. When $\Delta Z_{tip} = 25\%D$, the lift coefficient first increases, then decreases, and then continues to increase, finally reaching its peak when the angle of attack equals 22°. Figure 9(a) compares the influence of the lift coefficient of the distributed propulsion system ($C_{L, tot}$) and the wing lift coefficient (C_L) as the angle of attack and spanwise distance change. The lift coefficient of the distributed propulsion system is composed of the wing lift coefficient and the propeller lift (i.e., the thrust component perpendicular to the incoming flow direction). Figure 9(b) displays the lift coefficient intended to represent the influence of propeller-wing coupling on the wing lift coefficient, while Figure 9(b) aims to evaluate the overall lift gain of the distributed propulsion system. It can be observed that the thrust component of the propeller can compensate for the decrease in the wing lift coefficient at high angles of attack, resulting in minimal variation in the lift coefficient of the distributed thrust system at high angles of attack. Compared to the wing lift coefficient, the lift coefficient of the distributed propulsion system increases by a maximum of approximately 30%, and by a maximum of about 169% compared to a clean wing. This indicates that flight at high angles of attack better demonstrates the advantages of the distributed propulsion system.





(a) Wing lift coefficient (C_L)

(b) Distributed propulsion system lift coefficient ($C_{L, tot}$) Figure 9 Lift coefficient variation with ΔZ_{tip} under different angles of attack

To analyze the relationship between the spanwise distance of distributed propellers (ΔZ_{tip}) and the angle of attack in detail, the Figure 10 below demonstrates the pressure and flow field distributions of the distributed propulsion system under different ΔZ_{tip} and angle of attack conditions. According to the graph in Figure 9 and the analysis of the visualized flow field, within the scope of parameter research, the propeller-wing-flap interaction can be classified into three flow states: small spanwise distance ($\Delta Z_{tip} \le 10\%D$), medium spanwise distance ($\Delta Z_{tip} = 25\%D$), and large spanwise distance ($\Delta Z_{tip} = 100\%D$). In addition, the flow state corresponding to the change of angle of attack at different ΔZ_{tip} also undergoes significant changes. To better explain the flow mechanism on the wing surface, Figure 10 illustrates the flow diagrams at different angles of attack across different ΔZ_{tip} , summarizing the flow field and pressure distributions presented in Figure 11.

The flow mechanisms at low angles of attack across different ΔZ_{tip} are largely similar: On the ascending blade (P- side), the effective angle of attack of the wing increases, enhancing the suction peak at the leading edge of the wing and tilting the suction zone forward (reducing induced drag). On the descending blade (P+ side), the effective angle of attack of the wing decreases, weakening the suction peak, resulting in a backward tilt of the generated force (increasing induced drag). This pressure gradient leads to significant spanwise flow on the wing surface. The distributed propeller with a small ΔZ_{tip} restricts the escaped tip vortex flow, presenting a contracted state on the ascending blade (P-side), which intensifies as the angle of attack increases (as shown in Figure 11). The flow separation that occurs on a clean wing at high angles of attack disappears due to the presence of the distributed propeller.

At medium spanwise distance(ΔZ_{tip} =25%D), the coupling effect of the distributed propeller on the wing surface weakens. When the angle of attack is small, the flow on the suction side of the main wing exhibits a slightly expanded state. As the angle of attack increases, the flow on the suction side gradually contracts, and the high-pressure zone on the suction side surface moves from the suction side to the pressure side, thus increasing the low-pressure region on the suction side of the wing. It can be inferred that positioning the distributed propeller vertically lower should be beneficial for expanding the low-pressure region on the suction side of the wing.

At large spanwise distance($\Delta Z_{tip}=100\%D$), the area of the non-slipstream region increases, and the distributed propulsion coupling continues to weaken. The flow field on the wing surface becomes similar to that of an isolated propeller-wing configuration: The escaped wingtip vortex causes an expanded state on both sides of the propeller. Due to the propeller increasing the suction peak near the leading edge of the wing, the flow separation in the non-slipstream region occurs earlier compared to a clean wing. The separation vortex in the non-slipstream region rapidly develops along the leading edge of the wing under the influence of the distributed propeller. The propeller slipstream on both sides tends to contract due to the compression of the separation vortex. The large separation region significantly reduces the lift, but the lift generated at the same angle of attack is still higher than that of a clean wing. As shown in Figure 11, the flow over the flaps is also noteworthy. Because of the distributed propeller, the flaps exhibit a flow opposite to that of the main wing: The flow over the flaps on the descending blade (P+ side) presents a contracted state, resulting in a more pronounced and uniform low-pressure region at their leading edges, which is beneficial for increasing lift in a distributed propulsion system. The flow characteristics on the flap surfaces across different spanwise distance are similar, and this flow feature is more prominent at small spanwise distance. As the angle of attack increases, the lowpressure region gradually moves spanwise from the descending blade (P+ side) to the ascending blade (P- side), and the area of the low-pressure region decreases.

As shown in Figure 12, with the increase of the angle of attack, while flow separation does not occur on the surface of some configurations of the wing, the airflow behind the propeller is no longer able to adhere to the upper surface of the wing (this is also evident in the misalignment of the volume streamlines and surface streamlines in Figure 10). Instead, the propeller vortex is formed above the suction surface of the wing, resulting in a decrease in the lift coefficient of the distributed propulsion system.

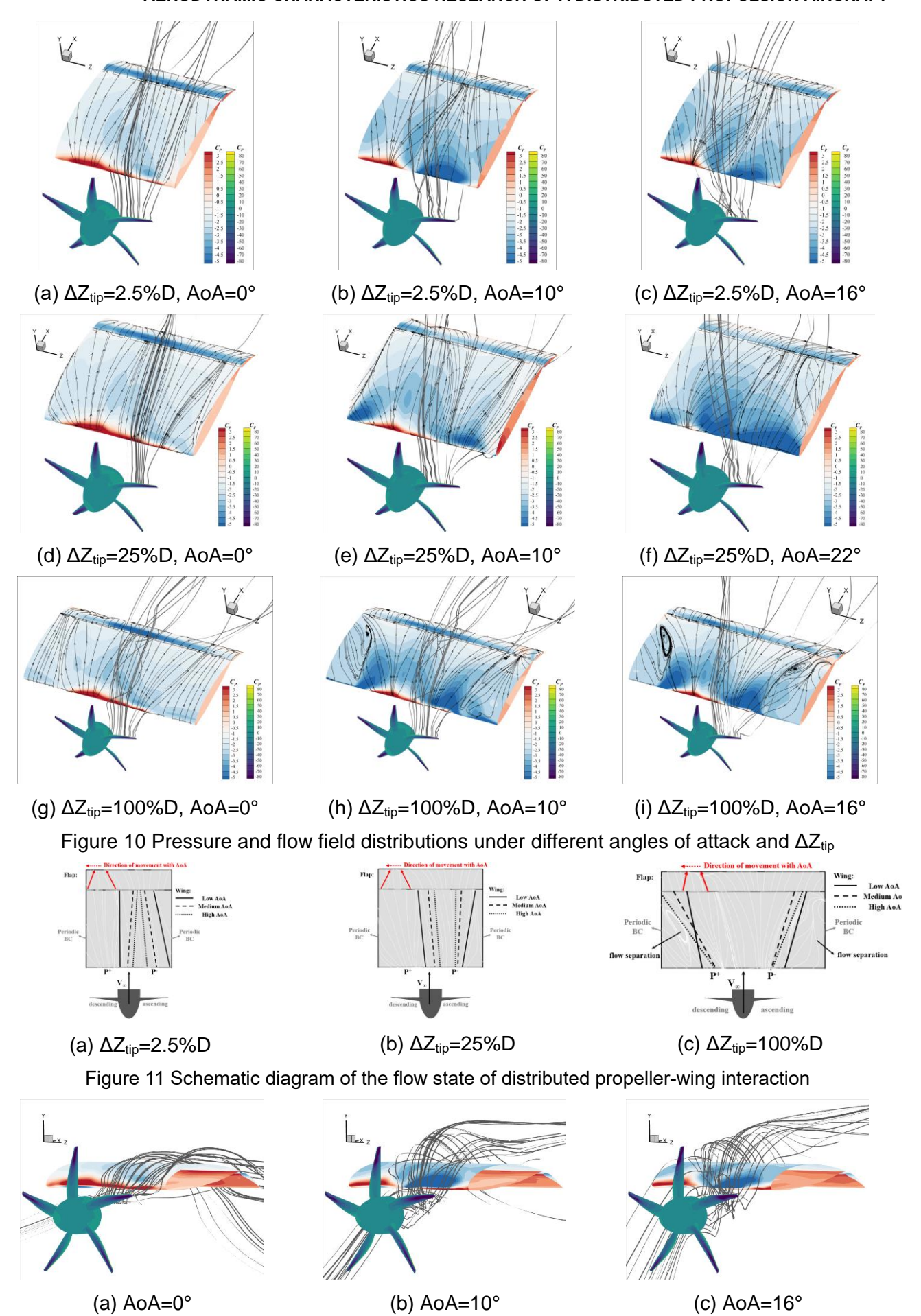


Figure 12 The streamline distribution on the suction side of the airfoil in the wake flow under different angles of attack

4. Conclusions

The present study utilizes the MRF (Multiple Reference Frame) method to investigate the relationship between spanwise distance(ΔZ_{tip}) and angle of attack in high-lift scenarios of distributed propulsion systems. The distributed propulsion system is simplified into an is infinite wing and an infinite number of propellers through the 2.5D approach. The results of the parametric study are used to guide the future optimization design of distributed propulsion systems. The study draws the following conclusions:

- (1) At low angles of attack, the propeller efficiency increases with the increase in spanwise distance. However, as the angle of attack increases, the propeller efficiency decreases with the increase in spanwise distance.
- (2) Distributed propellers with a smaller spanwise distance generate a large number of vortex structures at the blade tips, which can reduce the propeller efficiency.
- (3) The small spanwise distance enhances the lift-increasing effect of the distributed propulsion system. However, as the angle of attack increases, the incoming flow passing through the propeller gradually fails to adhere to the wing surface, resulting in a decrease in the wing's lift coefficient. In a particular case, at a high angle of attack when ΔZ_{tip}=25%D, the incoming flow directly interacts with the pressure side of the wing, positioning the P⁺ region at the leading edge of the wing's pressure side, while a low-pressure area emerges at the leading edge of the suction side. This condition favors an increase in lift. It can be speculated that there exists a coupling relationship between the vertical arrangement of the propeller and the spanwise distance of the distributed propeller, which will be further explored in subsequent studies.
- (4) The three different spanwise distance of the distributed propulsion system correspond to distinct aerodynamic characteristics, but all operating conditions exhibit an increase in lift compared to isolated wings, and the angle of attack for flow separation occurs earlier. In this scenario, the large spanwise distance will significantly reduce the lift-increasing effect of the distributed propulsion system.

5. Contact Author Email Address

First Author: suqichen97@163.com

Corresponding Author: guozheng@nudt.edu.cn

6. Copyright Statement

The authors confirm that they, and/or their company or organization, hold copyright on all of the original material included in this paper. The authors also confirm that they have obtained permission, from the copyright holder of any third party material included in this paper, to publish it as part of their paper. The authors confirm that they give permission, or have obtained permission from the copyright holder of this paper, for the publication and distribution of this paper as part of the ICAS proceedings or as individual off-prints from the proceedings.

References

- [1] Del Rosario R. Advanced concepts for aircraft LTO NOx reduction: A NASA Perspective. *Aircraft Noise and Emissions Reduction Symposium (ANERS)*, Marseille, France, 2011.
- [2] Kroo I. Propeller-wing integration for minimum induced loss. *Journal of Aircraft*, Vol. 23, No. 7, pp 561-565, 1986
- [3] Gohardani A.S. A synergistic glance at the prospects of distributed propulsion technology and the electric aircraft concept for future unmanned air vehicles and commercial/military aviation. *Progress in Aerospace Sciences*, Vol. 57, No. 2, pp 25-70, 2013.
- [4] Veldhuis L.L. Review of propeller-wing aerodynamic interference. 24th International Congress of the Aeronautical Sciences, Yokohama, Japan, 2004.
- [5] Veldhuis L.L. Optimization of tractor propeller/wing configurations. *Proceedings of the Institution of Mechanical Engineers, Part G: Journal of Aerospace Engineering*, Vol.209, No. 3, pp 215-226, 1995.
- [6] Veldhuis L.L. Propeller wing aerodynamic interference. 1st edition, Tu Deft, 2005.
- [7] Veldhuis L.L. Heyma P.M. Aerodynamic optimization of wings in multi-engined tractor propeller arrangements. *Aircraft Design*, Vol. 3, No. 3, pp 129-149, 2000.
- [8] Ameyugo G, Taylor M, Singh R. Distributed propulsion feasibility studies. 25th international congress of the aeronautical sciences, Hamburg, Germany, 2006.
- [9] Stoll A.M., Bevirt J, Moore M.D, et al. Drag reduction through distributed electric propulsion. *14th AIAA Aviation Technology, Integration, and Operations Conference*, Atlanta, Georgia, 2014.
- [10] Borer N.K, Derlaga J.M, Deere K.A, et al. Comparison of aero-propulsive performance predictions for distributed propulsion configurations. *55th AIAA Aerospace Sciences Meeting*, Grapevine, Texas, p. 0209, 2017.

- [11] Deere K.A, Viken S, Carter M, et al. Computational analysis of powered lift augmentation for the LEAPTech distributed electric propulsion wing. *AIAA Applied Aerodynamics Conference*, Denver, Colorado, 2017
- [12] Deere K A, Viken S, Carter M.B, et al. Computational component build-up for the X-57 Distributed electric propulsion aircraft. 2018 AIAA Aerospace Sciences Meeting, Kissimmee, Florida, 2018.
- [13] Stoll A. Comparison of CFD and experimental results of the LEAPTech distributed electric propulsion blown wing. *15th AlAA Aviation Technology, Integration, and Operations Conference*, Dallas, Texas, P. 3188, 2015.
- [14] YANG W, FAN Z L, WU W H, et al. Optimal design of distributed propeller layout considering slipstream effect. *Acta Aerodynamica Sinica*, Vol.39, No.3, pp 71-79, 2021.
- [15] Wang H, Gan W, Li D, An investigation of the aerodynamic performance for a propeller-aided lift-enhancing double wing configuration. *Aerospace Science and Technology*, Vol. 105, No. 105991, 2020.
- [16] Wang K L, Zhu X P, Zhou Z, et al. Distributed electric propulsion slipstream aerodynamic effects at low Reynolds number. *Acta Aeronautica et Astronautica Sinica*, Vol. 37, No. 9, pp 2669-2678, 2016.
- [17] Wang K L, Zhou. Aerodynamic design of tractor propeller for high-performance distributed electric propulsion aircraft. *Chinese Journal of Aeronautics*, Vol. 34, No. 10, pp 20-35, 2021.
- [18] Viken J K, Viken S, Deere K A, et al , Design of the cruise and flap airfoil for the X-57 Maxwell distributed electric propulsion aircraft. 35th AIAA Applied Aerodynamics Conference, Denver, Colorado, 2017.
- [19] Stokkermans T.C.A. Aerodynamics of propellers in interaction dominated flowfields: an application to novel aerospace vehicles, TU Delft, 2020.
- [20] Cusati V, Corcione S, Nicolos Fi. Improvement of take-off performance for an electric commuter aircraft due to distributed electric propulsion. *Aerospace*, Vol. 10, No. 3, 2023.
- [21] Wang. H B, Zhu X P, Zhou Z. Numerical simulation of the propeller/wing interactions at low Reynolds number. 30th Congress of the International Council of the Aeronautical Sciences, Daejeon, Korea, 2016.
- [22] Beckers M.F, Schollenberger M, Lutz T. Numerical investigation of high-lift propeller positions for a distributed propulsion system. *Journal of Aircraft*, Vol. 0, No. 0, pp-1-12, 2022.
- [23] Gothow A, Weiss J, Bardenhagen A. Experimental parameter study of distributed electric propulsion on a 2D wing model in high-lift configuration. *AIAA AVIATION 2023 Forum*, San Diego, California, 2023.
- [24] Ciliberti D, Della Vecchia P, Orticalco V. Aero-Propulsive interactions between UAV wing and distributed propellers due to their relative position. *Drones*, Vol. 7, No. 1, 2023.
- [25] Rosa D, Morales Tirado E, Mingione G. Parametric investigation of a distributed propulsion system on a regional aircraft. *Aerospace*, Vol. 9, No. 4, 2022.
- [26] Resende G.J, Malatesta V, Savio M.C. Wing's aerodynamic characteristics due to distributed propulsion over the wingspan. *Journal of the Brazilian Society of Mechanical Sciences and Engineering*, Vol. 45, No. 9, p. 495, 2023.
- [27] Wang K L, Zhou Z, Zhu X P. Aerodynamic design of multi-propeller/wing integration at low Reynolds numbers. *Aerospace Science and Technology*, Vol. 84, pp 1-17, 2017.
- [28] Wang S S, Guo Z. Design, optimization and application of two-element airfoils for tactical UAV. *Advances in Mechanical Engineering*, Vol. 14, No. 11, 2022.
- [29] Sinnige T, Arnhem N V,. Stokkermans T.C.A. Wingtip-Mounted propellers: aerodynamic analysis of interaction effects and comparison with conventional layout. *Journal of Aircraft*, Vol. 56, No. 1, pp 295-312, 2019.